Robust Guidance for Electro-Optical Missiles

PINI GURFIL
Princeton University

A robust guidance law is presented which renders zero miss distance (ZMD) against deterministically or randomly maneuvering targets for all missile parametric uncertainties. Since the resulting guidance controller is a phase-lead network, it is mainly suitable for systems characterized by moderate glint levels such as electro-optical missiles. The structured uncertainties in missile dynamics are modeled by interval transfer functions. It is first shown that for the nominal case, when the total missile transfer function is positive real, ZMD can be obtained. When uncertainties are considered, the problem becomes design of a guidance controller which renders a family of transfer functions positive real. A new algorithm for the design of such controllers is proposed. An example illustrating a typical design procedure for a nonlinear real-life missile model is given, showing the simplicity and effectiveness of the proposed robust guidance. The main conclusion of this work is that the newly developed guidance law performs well against highly maneuvering targets and may be a suitable alternative to optimal guidance laws in low-glint systems.

Manuscript received May 30, 2001; revised February 3, 2003; released for publication February 26, 2003.

IEEE Log No. T-AES/39/2/813088.

Refereeing of this contribution was handled by T. F. Roome.

Author's address: Dept. of Mechanical and Aerospace Engineering, Princeton University, J228 Engineering Quad, Princeton, NJ 08544, E-mail: (pgurfil@princeton.edu).

I. INTRODUCTION

Modern missiles operate over a wide range of flight conditions, which vary with altitude, Mach number, angle-of-attack, and engine thrust. The mechanical characteristics of the airframe, such as the center of gravity, change as well. In addition to these changes, missile aerodynamic and mechanical properties for a given flight condition are often uncertain to some extent. An engineering effort is usually made to incorporate these uncertainties into the aerodynamic and mechanical models and compensate the dynamical behavior of the missile using both a robust autopilot and a robust guidance law. This work focuses on the latter issue. This stems mainly from the fact that, eventually, the main objective is to achieve small miss distance. This stresses the importance of synthesizing a simple robust guidance methodology aimed at achieving small miss distance given the model of uncertainty. We discuss structured parametric uncertainties of the interval type. This uncertainty model is the most useful from the engineering practice standpoint.

Previous attempts to synthesize robust guidance laws for missiles with parametric uncertainties were reported in the literature. In some cases, only a single uncertain time constant was considered [1, 2]. This, of course, constitutes a considerable simplification of the problem, since real-life models include high-order transfer functions having multiple poles and zeros. Others have employed H_∞ theory assuming either nonlinear kinematics [3] or, again, simplified linear models [4]. The resulting guidance laws obtained in [3, 4] were complex, giving little engineering insight. Thumb-rules, aimed at modification of linear-quadratic optimal guidance to account for parametric uncertainties were also considered [5]. The latter approach requires estimation of target maneuver and time-to-go, which by themselves deteriorate the overall robustness of the guidance law. A discussion on robustness of linear quadratic optimal guidance can be found in [23–26].

An alternative approach is proposed here to the synthesis of robust guidance. The suggested methodology is based upon recent works, that have utilized the method of adjoints [6] and the small gain theorem [7] to prove that when the overall linearized missile dynamics is positive-real (PR), zero miss distance (ZMD) can be obtained against targets performing any (bounded) deterministic or random maneuver. References [6, 7] have adopted the linearized time-varying framework of proportional navigation guidance (PNG) to prove the main result. Hence, the resulting guidance law was called ZMD-PNG. In this study, we expand the ZMD-PNG law to deal with parametric uncertainties associated with any arbitrary order missile dynamics.

To this end, we use some important theoretical results that establish PR of interval transfer functions [8]. Based on theses results, a new algorithm rendering a given family of interval transfer functions robustly PR is proposed. The most powerful outcome of this methodology is a robust ZMD-PNG guidance law, i.e. a guidance law that achieves ZMD for any (bounded) target maneuver even when the missile transfer function contains parametric uncertainties.

A thorough performance analysis of the newly developed robust guidance law is provided using a realistic, nonlinear stochastic model of an electro-optical missile. The performance of the robust ZMD-PNG is compared with an optimal guidance law, showing promising performance with moderate levels of glint.

The paper is organized as follows. In Section II, some mathematical preliminaries are presented. Section III presents the guidance model and associated uncertainties. Section IV derives the robust guidance law. Section V proposes an algorithm for the design of robust PR transfer functions. Section VI considers an illustrative example. In Section VII some conclusions are drawn.

II. MATHEMATICAL PRELIMINARIES

The purpose of this section is to present some mathematical preliminaries that are utilized in the sequel. First, the concept of PR functions is defined. Then, the mathematical formulation of parametric uncertainties is explained.

Consider the rational transfer function

$$H(s) = N(s)/D(s) \tag{1}$$

where

$$N(s) = \sum_{i=0}^{m} n_i s^i, \qquad D(s) = N(s) = \sum_{i=0}^{q} d_i s^i, \qquad n_i, d_i \in \Re \tag{2}$$

DEFINITION 1 The transfer function $H(s)$ is PR if

$$\mathrm{Re}[H(s)] \geq 0 \qquad \forall \quad \mathrm{Re}[s] \geq 0. \tag{3}$$

The following theorem provides necessary and sufficient condition for PR.

THEOREM 1 *The transfer function $H(s)$ is PR if and only if*

a) *$H(s)$ is a stable transfer function.*

b) *The poles of $H(s)$ on the imaginary axis are distinct and the associated residues are real and nonnegative.*

c) $\mathrm{Re}[h(j\omega)] \geq 0 \ \forall \omega \geq 0$.

The class of PR functions will be denoted $\{PR\}$. Note that a useful property of PR functions is as follows.

PROPERTY 1 *A necessary condition for $H(s)$ to be PR is that the relative degree $r = |q - m|$ does not exceed* 1.

We deal hereafter with structured parametric uncertainties of the interval type; that is, it is assumed that both $N(s)$ and $D(s)$ constitute interval polynomials. To this end, we introduce interval polynomials and some related notation.

An interval family of polynomials $\mathcal{P}$ is a set of polynomials

$$\Delta(s) = \sum_{i=0}^{p} \delta_i s^i \tag{4}$$

where the coefficients vector $\delta = [\delta_0, \delta_1, \ldots, \delta_p]^T$ belongs to a given uncertainty hyperrectangular domain B_δ in the coefficient space,

$$B_\delta = \{\delta \in \Re^{p+1} : \delta_i^- \leq \delta_i \leq \delta_i^+, \ i = 0, 1, \ldots, p\}. \tag{5}$$

The parametric uncertainties of the transfer function $H(s)$ (see (1)) are modeled by an interval family of proper plants $\mathcal{H}$, given by

$$H(s;n,d) = N(s;n)/D(s;d) \tag{6}$$

where $N(s;n)$ and $D(s;d)$ are interval polynomials with coefficient vectors $n = [n_0, n_1, \ldots, n_m]^T$, $d = [d_0, d_1, \ldots, d_q]^T$ $(m \leq q)$ lying in hyperrectangular domains B_n and B_d, as defined in (5), in the numerator and denominator coefficient spaces, respectively.

DEFINITION 2 An interval family of proper plants $\mathcal{H}$ (6) is robustly PR if any member of $\mathcal{H}$ is PR.

We conclude the mathematical preliminaries by introducing four important polynomials of the interval family $\mathcal{P}$, known as the Kharitonov polynomials [9]. These polynomials constitute a subset of the corner polynomials associated with B_δ, and are defined as follows:

$$\begin{aligned}
\Delta_{++}(s) &\triangleq \delta_0^+ + \delta_1^+ s + \delta_2^- s^2 + \delta_3^- s^3 + \cdots \\
\Delta_{--}(s) &\triangleq \delta_0^- + \delta_1^- s + \delta_2^+ s^2 + \delta_3^+ s^3 + \cdots \\
\Delta_{+-}(s) &\triangleq \delta_0^+ + \delta_1^- s + \delta_2^- s^2 + \delta_3^+ s^3 + \cdots \\
\Delta_{-+}(s) &\triangleq \delta_0^- + \delta_1^+ s + \delta_2^+ s^2 + \delta_3^- s^3 + \cdots .
\end{aligned} \tag{7}$$

III. GUIDANCE MODEL AND ASSOCIATED UNCERTAINTIES

The derivation of the suggested robust guidance law requires the presentation of the intercept kinematics and associated assumptions. To this end, the framework of the well-known PNG is adopted. The general formulation of a three-dimensional PNG is rather complicated; however, by assuming that the lateral and longitudinal maneuver planes are decoupled by means of roll control, one can deal with the equivalent two-dimensional problem in quite a realistic manner. Thus, it is assumed hereafter that

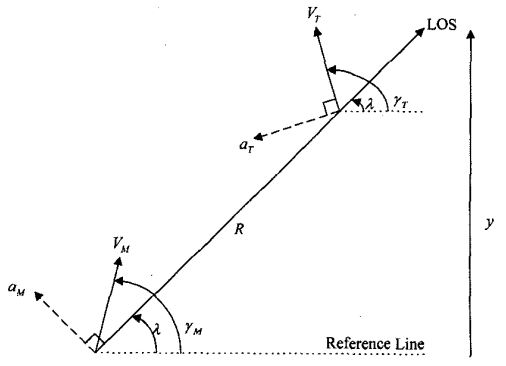

Fig. 1. Intercept geometry.

the geometry is two-dimensional. This assumption renders the planar interception missile-target geometry depicted in Fig. 1. This figure describes a missile employing PNG to intercept a maneuvering target.

Based on Fig. 1, a linearized model of the guidance dynamics can be developed. Such a model is widely used in the analysis of PNG [10–14]. A block diagram describing the linear model is given in Fig. 2. In this linear time-varying system, missile acceleration a_M is subtracted from target acceleration a_T to form a relative acceleration $\ddot{y}$. A double integration yields the relative vertical position y (see Fig. 1), which at the end of the engagement $t = t_f$, is the miss distance $y(t_f)$. By assuming that the closing velocity V_C is constant, the relative range is given by

$$R(t) = V_C \cdot t_{\text{go}} \tag{8}$$

where t_{go} is the time to go, defined as $t_{\text{go}} \triangleq t_f - t$. Dividing the relative vertical position y by the range given in (8), yields the geometric line-of-sight (LOS) angle λ. The missile seeker is represented in Fig. 2 as an ideal differentiator with an additional transfer function $G_1(s)$, representing the LOS measurement and noise filtering dynamics. The seeker generates a LOS rate command $\dot{\lambda}_m$, which is multiplied by the proportional navigation (PN) gain $N' \cdot V_C$ to form a commanded missile maneuver acceleration a_C, with N' being the effective PN constant.

The flight control system, whose dynamics are represented by the transfer function $G_2(s)$, attempts to adequately maneuver the missile to follow the desired acceleration command.

The transfer functions $G_1(s)$ and $G_2(s)$ constitute the so-called total guidance transfer function, defined as

$$H(s) \triangleq \frac{G_1(s)G_2(s)}{s}. \tag{9}$$

Based on the linear PNG model, recent studies have utilized the method of adjoints [6] and the small gain theorem [7] to rigorously prove the following important theorem.

THEOREM 2 *Let the missile maneuver acceleration a_M and be limited, $|a_M| \le a_{M_{\max}}$, and the target acceleration be bounded, $|a_T| \le a_{T_{\max}}$. Denote $\mu_0 = a_{M_{\max}}/a_{T_{\max}}$. If there exists a transfer function $K(s)$, called the guidance controller, such that $K(s)H(s) \in \{PR\}$, and in addition $N' \ge 2\mu_0/(\mu_0 - 1)$, then $y(t_f) = 0\ \forall t_f$, $\forall |a_T| \le a_{T_{\max}}$.*

The guidance law derived from Theorem 2 has been called ZMD-PNG. When the parameters of $H(s)$ are known exactly, a suitable controller $K(s)$ can be designed such that $K(s)H(s) \in \{PR\}$ and the ZMD-PNG law yields indeed small miss distance [7]. However, in the bulk of practical applications, system parameters lie within some prespecified interval. This uncertainty affects the performance of ZMD-PNG, and prevents the attainment of ZMD. In the next section, a robust ZMD-PNG law is derived, such that ZMD is obtained for interval uncertainties.

IV. DERIVATION OF ROBUST ZMD-PNG

Assume that the total guidance transfer function $H(s)$ (eq. (9)) and its associated parametric uncertainties, constitute a family of proper interval plants $\mathcal{H}$, defined as in (6). For the synthesis of a robust ZMD-PNG law, it is required to find a guidance controller $K(s)$ such that the family $\mathcal{H}_K$, defined by

$$H_K(s;\hat{n},\hat{d}) = K(s)N(s;n)/D(s;d) = \hat{N}(s;\hat{n})/\hat{D}(s;\hat{d}) \tag{10}$$

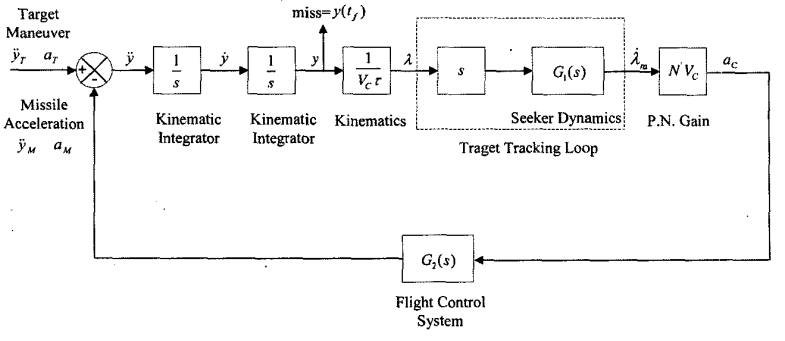

Fig. 2. Linearized PNG model block diagram.

is robustly PR (see Definition 2). The problem of robust PR has been addressed in many studies [8, 15, 16]. The most up-to-date result states that robust PR of $\mathcal{H}_K$ can be inferred by PR of eight extremal transfer functions of the family [8]. This result is summarized in the following theorem.

THEOREM 3 *An interval family $\mathcal{H}_K$ of proper transfer functions is PR if and only if the following eight transfer functions are PR:*

$$H_1(s) = \hat{N}_{+-}(s)/\hat{D}_{--}(s), \qquad H_2(s) = \hat{N}_{--}(s)/\hat{D}_{+-}(s) \tag{11}$$

$$H_3(s) = \hat{N}_{++}(s)/\hat{D}_{+-}(s), \qquad H_4(s) = \hat{N}_{+-}(s)/\hat{D}_{++}(s) \tag{12}$$

$$H_5(s) = \hat{N}_{-+}(s)/\hat{D}_{++}(s), \qquad H_6(s) = \hat{N}_{++}(s)/\hat{D}_{-+}(s) \tag{13}$$

$$H_7(s) = \hat{N}_{--}(s)/\hat{D}_{-+}(s), \qquad H_8(s) = \hat{N}_{-+}(s)/\hat{D}_{--}(s). \tag{14}$$

The following corollary [8] simplifies the conditions for PR of low-order interval families.

COROLLARY 1 *Given an interval family $\mathcal{H}_K$ of proper transfer functions,*

a) *If $q = 2$, PR of the two transfer functions* (11) *implies PR of the entire family.*

b) *If $q = 3$, PR of the four transfer functions* (11), (12) *implies PR of the entire family.*

c) *If $q = 4$, PR of the six transfer functions* (11)–(13) *implies PR of the entire family.*

Thus, our objective is to design a guidance controller $K(s)$ such that the conditions for PR stated in Theorem 1 are satisfied. Given an interval family $\mathcal{H}_K$ as in (10), such a controller might be

$$K(s) = \prod_{i=1}^{q-m-1} (c_i s + 1), \qquad c_i > 0 \quad \forall \quad i. \tag{15}$$

Selection of a controller of the form (15) stems from a practical standpoint. First, it is assured that (15) is a Hurwitz polynomial; thus controllers rendering right-half plane zeros (which prevents from $\mathcal{H}_K$ to be robustly PR) are not considered. This property is important when performing a parametric optimization controller design as suggested in the next section, since it reduces the number of iterations required to derive an appropriate solution. Second, this controller is merely a cascade of proportional-derivative (PD) prefilters, that can be easily implemented, without changing the existing predesigned dynamic properties of $G_1(s)$ and $G_2(s)$. For practical purposes, it may be required to add a high-frequency roll-off. This issue and its effect on the robustness properties is discussed in Section VI.

Notice that due to Property 1, the order of the controller (15) should be $q - m - 1$. This is because $G_1(s)$ and $G_2(s)$ represent the closed-loop dynamics of the seeker and flight control system, respectively, and are thus strictly proper. In order for Property 1 to hold, it is necessary to design a controller which yields $r[K(s)G_1(s)G_2(s)] = 0$ and $r[K(s)G_1(s)G_2(s)/s] = r[K(s)H(s)] = 1$ (when ruling out design of nonproper transfer functions). In the next section, an algorithm for designing a robust PR controller is suggested.

V. ALGORITHM FOR THE DESIGN OF ROBUST PR TRANSFER FUNCTIONS

Several results concerning the design of robust PR transfer functions have been reported in the literature [17–19]. However, the design procedures suggested in these studies have some major flaws. The most significant one is that usually only denominator plants were considered. This means that these algorithms do not offer a suitable solution to a general dynamics having multiple zeros and multiple poles. Furthermore, the sufficient conditions derived for designing PR transfer functions often result in a linear programming problem, which requires a numerical solution [17]. Moreover, to simplify the treatment, the existing studies [15, 18, 19] offered controllers that render a given transfer function robustly PR with $r[K(s)H(s)] = 0$ which is not suitable for our case ($r[K(s)H(s)] = 1$). Consequently, we might as well solve this problem using numerical methods to begin with, instead of going through a tedious analytical study. We thus propose a simple algorithm for the design of robust PR transfer functions. This new algorithm is essentially a constrained direct parameter optimization procedure, which can be easily solved using numerical optimization techniques.

The algorithm comprises the following stages. Let

$$c = [c_1, c_2, \ldots, c_{q-m-1}]^T. \tag{16}$$

Also, define

$$[h_K(\omega, c)]_i = \mathrm{Re}\left\{ \left[\prod_{l=1}^{q-m-1} (c_l j\omega + 1) \right] H_i(j\omega) \right\}, \qquad i = 1,2,\ldots,8 \tag{17}$$

with the extremal transfer functions given in (11)–(14).

The objective is to find

$$c^* = \arg\min_c c^T c \tag{18}$$

subject to

$$\min_\omega [h_K(\omega, c)]_i \geq 0, \qquad i = 1,2,\ldots,8 \tag{19}$$

where the constraints (19) are based on the necessary and sufficient conditions for robust PR stated in

Theorem 2. The number of constraints can be reduced for low-order dynamics (Corollary 1).

The selection of the quadratic cost function (18) stems mainly from the following reasoning. The purpose is to design a robust PR transfer function with the minimal phase lead possible. Thus, problems associated with high-bandwidth control, such as amplification of measurement noise, are reduced. Thus, since

$$\arg[K(j\omega)] = \arg\left[\prod_{i=1}^{q-m-1}(c_i j\omega + 1)\right] = \sum_{i=1}^{q-m-1}\arg(c_i j\omega + 1) \tag{20}$$

a minimization of each parameter c_i (subject to (19)) is required in order to obtain the minimal phase lead. This consideration establishes the particular selection of the quadratic cost (18). An example illustrating the design of a robust guidance law for a real-life missile model using the suggested algorithm is considered next.

Finally, note that minimization of (18) subject to (19) may reach a local minimum; however, it is not the purpose of the algorithm nor the goal of the robust guidance method to find the global minimum. The key point is that any solution, even a local optimum, suffices. This is due to the fact that in order to find a robust guidance controller, which renders the total dynamics robustly PR, only the constraints (19) should be satisfied. The cost functional (18) was added merely to find a candidate solution that gives small phase lead, not necessarily the smallest phase lead. The noise filtering system should be designed separately.

VI. ILLUSTRATIVE EXAMPLE

In the previous sections, a robust guidance law, ZMD-PNG, was synthesized. The purpose of this section is to investigate the performance of ZMD-PNG when implemented in a real-life canard-steered electro-optical missile. Furthermore, a detailed comparison between ZMD-PNG, optimal guidance law (OGL), and the classical PNG is given. The comparison includes both deterministic simulation runs and a Monte-Carlo analysis.

The missile models used here are believed to constitute a faithful representation of a large family of electro-optical guided missiles. The real-life models include a detailed flight control system, described in Appendix A, which consists of an aerodynamic model, fin actuators and sensors, and an electro-optical tracking loop, which includes a detailed model of the seeker and tracker. Both the flight control system and the tracking loop include nonlinear effects such as state saturation and field-of-view (FOV) limits. Exogenous disturbances such as fin bias and measurement noise are modeled as well. It should be stressed that due to the inherent phase lead, the proposed guidance method is mainly suitable for electro-optical missiles, where the glint noise is usually range independent and more moderate than in RF systems.

A. Guidance Law Synthesis

In order to design a robust ZMD-PNG law, transfer functions of the flight control system, $G_2(s) = a_M(s)/a_C(s)$, and the tracking loop, $G_1(s) = \dot{\lambda}_m/\dot{\lambda}$, are required. These transfer functions can be found in two steps. First, the nonlinear terms are left out. Second, the resulting high-order linear models are reduced using state truncation method such as balanced realization. It is important to stress that this procedure is used for the guidance design only, not for the overall performance evaluation of the missile, where the complete, detailed nonlinear stochastic models are used.

We start with model reduction of the complex flight control system, described in Appendix A, which has 9 zeros and 13 poles. Using balanced realization state truncation, and the parameter values given in Appendix C, the following reduced-order transfer function is obtained

$$G_2(s) \approx \frac{\tau_2 s + 1}{s^2/\omega_n^2 + 2\zeta s/\omega_n + 1} \tag{21}$$

with the parameters lying in the intervals

$$\begin{aligned} 0.3 \le \tau_2 \le 0.4 \\ 30 \le \omega_n \le 40 \\ 0.2 \le \zeta \le 0.4. \end{aligned} \tag{22}$$

The simplified model (21) constitutes an adequate approximation to the overall flight control system dynamics, both in the frequency and time domains. It is subsequently used for ZMD-PNG design.

The tracking loop overall transfer function $G_1(s)$ is obtained in a similar manner. Using the numerical values of Appendix C, neglecting the FOV saturation and the pure tracking delay, we have

$$G_1(s) \approx \frac{1}{\tau_1 s + 1} \tag{23}$$

with $\tau_1 = 0.1$.

In (23), we neglected the influence of the seeker natural frequency uncertainty on the uncertainty of τ_1 due to the fact that $2 \cdot \zeta_{\text{seeker}}/\omega_{n_{\text{seeker}}} \gg \tau_1$. The overall transfer function of the guidance loop is therefore:

$$H(s) = G_1(s)G_2(s)/s = \frac{\tau_2 s + 1}{s(0.1s + 1)\cdot(s^2/\omega_n^2 + 2\zeta s/\omega_n + 1)}. \tag{24}$$

Following (15), the guidance controller chosen is

$$K(s) = (c_1 s + 1)(c_2 s + 1) \tag{25}$$

such that

$$H_K(s;n,d) = \frac{n_3 s^3 + n_2 s^2 + n_1 s + n_0}{d_4 s^4 + d_3 s^3 + d_2 s^2 + d_1 s + d_0} \tag{26}$$

with

$$\begin{aligned}
&0.3c_1c_2 \le n_3 \le 0.4c_1c_2 \\
&c_1c_2 + 0.3(c_1 + c_2) \le n_2 \le c_1c_2 + 0.4(c_1 + c_2) \\
&c_1 + c_2 + 0.3 \le n_1 \le c_1 + c_2 + 0.4 \\
&n_0 = 1 \\
&0.0000625 \le d_4 \le 0.000111 \\
&0.0016 \le d_3 \le 0.0031 \\
&0.11 \le d_2 \le 0.1267 \\
&d_1 = 1 \\
&d_0 = 0.
\end{aligned} \tag{27}$$

The parameter optimization problem becomes:
Find

$$[c_1^*, c_2^*]^T = \arg\min_{c_1,c_2}(c_1^2 + c_2^2) \tag{28}$$

subject to (note that only 6 constraints are required)

$$\min_{\omega}[h_K(\omega, c_1, c_2)]_i \ge 0, \qquad i = 1,2,\ldots,6. \tag{29}$$

The optimal parameters, rendering robust PR, were obtained using the MATLAB® Optimization Toolbox. We started with the initial guesses $c_1 = 0.2$, $c_2 = 0.8$. After 33 iterations, the optimization converged successfully, yielding $c_1 = c_2 = 0.2304$, that is

$$K(s) = (0.2304s + 1)^2. \tag{30}$$

Table I describes the iterative process generated by the optimization procedure. Assuming that the missile-target maneuver ratio satisfies $\mu_0 = 2$, forces the choice $N' \ge 4$ (see Theorem 2). We chose $N' = 5$. In addition, we must use a high-frequency roll-off to reject noise. From our experience and as shown in the simulations, a small roll-off has no influence whatsoever on the robustness of the guidance law. We placed the roll-off poles at $s = -100$, so the overall guidance law becomes

$$a_C = 5 \cdot V_C \frac{(0.2304s + 1)^2}{(0.01s + 1)^2}\dot{\lambda}_C. \tag{31}$$

This guidance law will yield (approximately) ZMD for the uncertain missile dynamics considered here.

The performance of the guidance law (31) is compared with OGL and the classical PNG. The

TABLE I
Convergence of Parameter Optimization Algorithm

Iteration #	c_1	c_2	Cost	Minimum of Constraints Vector (20)
1	0.2	0.8	0.68	0.02056
7	0.2169	0.4	0.2071	0.05375
10	0.2643	0.1131	0.0826	−0.136303
14	0.1360	0.1462	0.0398	−0.168842
17	0.1981	0.1849	0.0734	−0.043247
20	0.2219	0.2112	0.0938	−0.010729
23	0.2313	0.2261	0.1046	−0.00132
26	0.2316	0.2292	0.1061	2.61E-06
29	0.2312	0.2296	0.1061	−5.43E-07
32	0.2304	0.2304	0.1061	−2.19E-06
33	0.2304	0.2304	0.1061	0

commanded OGL maneuver acceleration is [2]

$$a_C = N'(\xi)[y + \dot{y}\hat{t}_{go} + 0.5\hat{a}_T\hat{t}_{go}^2 - a_M\tau_D^2(e^{-\xi} + \xi - 1)]/\hat{t}_{go}^2 \tag{32}$$

$$N'(\xi) = \frac{6\xi^2(e^{-\xi} + \xi - 1)}{2\xi^3 - 6\xi^2 + 6\xi + \xi - 12\xi e^{-\xi} - 3e^{-2\xi}}$$

where $\hat{t}_{go}$ is the estimated time-to-go, $\hat{a}_T$ is the estimated target maneuver, τ_D is the so-called "design" time constant, and $\xi \triangleq \hat{t}_{go}/\tau_D$. Due to the fact that the common OGL was originally conceived for first-order dynamics, there is a considerable mismatch between actual missile dynamics and the OGL. To deal with this mismatch, it was suggested [5] to use a "design" time constant τ_D which is about 1.5 times larger than the equivalent time constant of the system. In our case, the equivalent time constant is 0.66 s, so $\tau_D = 1$ s. It is also assumed that the time-to-go is estimated exactly, i.e. $\hat{t}_{go} = t_{go}$. For the estimation of target maneuver, the following model was adopted [20]:

$$\hat{a}_T = e^{-s\tau_a} \cdot a_T. \tag{33}$$

In (33) it is assumed that the target maneuver estimator constitutes a pure time delay of τ_a seconds. We chose $\tau_a = 0.2$ s, which is a rather optimistic value, since often the estimation delay is even larger.

The PNG design is far simpler. The sole degree-of-freedom is N'. We chose $N' = 5$, so that with PNG we have

$$a_C = 5 \cdot V_C \cdot \dot{\lambda}_m. \tag{34}$$

The target maneuver simulated to test the performance of the three guidance laws was a random phase sinusoidal maneuver. As noted in recent literature [21] one of the most challenging problems faced by a homing missile is the interception of ballistic missiles on atmosphere reentry. In this case, the target performs a so-called barrel-roll maneuver. A projection of this maneuver on the plane yields a sinusoidal target acceleration time history. In addition,

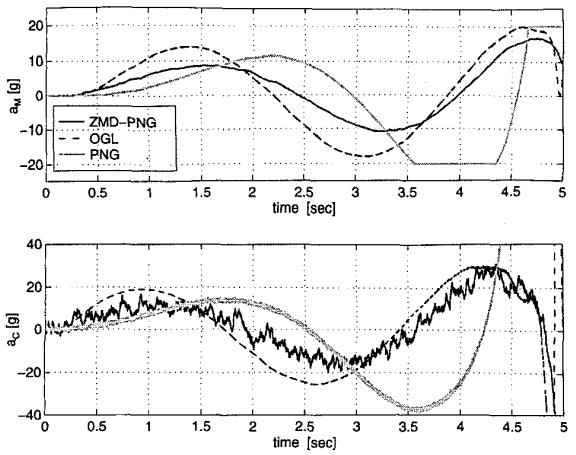

Fig. 3. Comparison of actual and commanded missile acceleration shows that ZMD-PNG requires less maneuver effort than OGL and PNG.

the starting time of the maneuver is unknown; it can be initiated at any given time point within the flight time of the interceptor. Thus, the target maneuver can be described by

$$a_T(t) = a_{T_0} \sin(\omega_T t + \phi) \tag{35}$$

where a_{T_0} is the maneuver magnitude, ω_T is the frequency, and ϕ is the phase, assumed uniformly distributed between 0 and 2π, which is completely equivalent to a random maneuver initiation time. In this example, the numerical values chosen where $a_{T_0} = 10g$ and $\omega_T = 1.7$ rad/s (this frequency is the optimal avoidance frequency for $N' = 5$).

B. Guidance Law Performance

The performance of the robust ZMD-PNG, PNG, and OGL against the random phase sinusoidal target maneuver includes both deterministic simulation runs and a Monte-Carlo analysis.

In the deterministic examination, all the parameters are kept in their nominal values (see Appendix C). The simulation was performed using the full nonlinear stochastic models described previously. For the deterministic case only, a constant flight time $t_f = 5$ s, and a constant target maneuver phase $\phi = 0$, were chosen. The time histories of the actual and commanded accelerations for $V_C = 1000$ m/s are depicted in Fig. 3.

Evidently, both ZMD-PNG and OGL yield superior performance comparing with PNG. Note that with PNG, the actual maneuver acceleration saturates 1.5 s before impact, which seriously increases the miss distance. However, with ZMD-PNG this saturation is avoided and the miss distance is much smaller. Note also that ZMD-PNG requires a smaller maneuver effort than OGL, because the OGL used here is actually suboptimal due to the high-order system dynamics.

As seen in Fig. 3, the acceleration command generated by ZMD-PNG is somewhat noisy. The noise level reaches $\pm 1g$ at $\pm\sigma$, which is feasible, and has no substantial implications on the performance of the system. The three guidance laws examined yielded the following miss distance:

$$\begin{aligned} y(t_f)|_{\text{ZMD-PNG}} &= -0.108 \text{ m} \\ y(t_f)|_{\text{OGL}} &= 0.114 \text{ m} \\ y(t_f)|_{\text{PNG}} &= 60.2 \text{ m}. \end{aligned} \tag{36}$$

Thus, while ZMD-PNG and OGL render a similar miss distance, PNG induces a considerably larger miss. This implies that PNG cannot deal adequately with sinusoidal targets, as was also mentioned in [11, 21].

We proceed with a thorough statistical examination of the guidance laws performance using a Monte-Carlo technique. In each simulation run, parameter values, as well as the seed used to generate the noise signals, are randomly selected according to prespecified probability distribution functions. After a large database of simulation runs has been created, the results, especially the miss distance, are statistically analyzed.

In this example, each simulation run used random parameter values (based upon the data given in Appendix C) and a random target maneuver phase. For each flight time, 300 simulation runs were performed. The procedure was repeated for flight times ranging from 2 s to 10 s. In order to evaluate miss distance statistics, the mean value of the absolute miss distance, defined by

$$\bar{y}(t_f) = \frac{1}{300} \sum_{i=1}^{300} |y(t_f)|_i \tag{37}$$

were examined. In addition, standard deviations of miss distance for each flight time was considered. The results are depicted in Figs. 4 and 5. Fig. 4 compares the mean value of absolute miss distance, and Fig. 5 compares the standard deviation of miss distance. PNG was not considered here because the deterministic examination showed that it yielded miss distance which was larger than the miss obtained with ZMD-PNG and OGL by an order-of-magnitude.

Clearly, ZMD-PNG yields smaller mean and rms miss than OGL. This is true for all flight times greater than 2 s. Moreover, with ZMD-PNG the miss distance is more robust to variations in flight times and in missile parameters. These observations imply that the newly developed guidance law can deal adequately with highly maneuvering targets. This merit is achieved with neither estimating target maneuver nor estimating time-to-go.

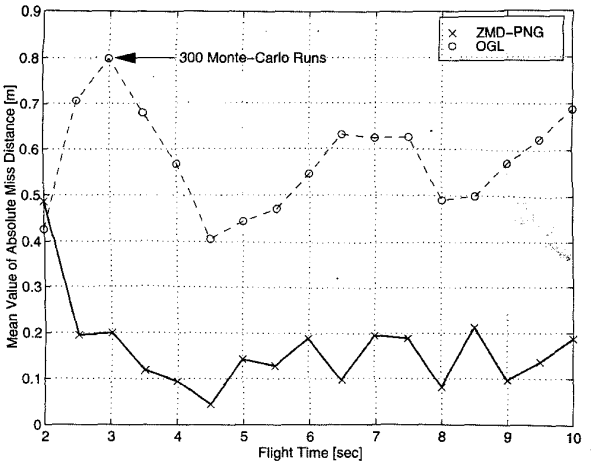

Fig. 4. Mean values of absolute miss distance with ZMD-PNG smaller than with OGL.

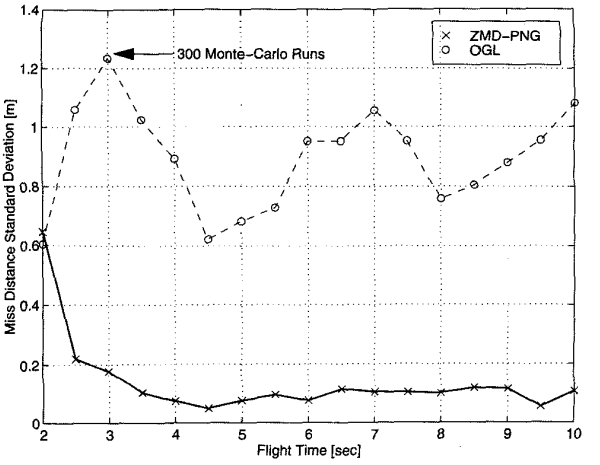

Fig. 5. Standard deviations of miss distance with ZMD-PNG smaller than with OGL.

Fig. 6 compares the energy expenditure measure, $E\{\int a_M^2\}$, for ZMD-PNG and OGL. Clearly, it is seen that ZMD-PNG requires less energy than OGL. This means that the induced drag of the missile will be smaller and the firing envelope wider. The difference between ZMD-PNG and OGL performance in this context is due to the fact that the OGL tested here is only suboptimal, due to the model mismatch previously mentioned. An OGL designed while taking into account the real high-order dynamics and saturations will out perform ZMD-PNG in terms of energy expenditure.

VII. SUMMARY AND CONCLUSIONS

This paper presented a robust guidance law that accounted for structured parametric uncertainties of the interval type. The new guidance law constituted an extension to the ZMD-PNG. In the nominal case, ZMD-PNG required the design of a controller which makes a given system dynamics PR. When uncertainties are considered, the controller should yield a family of PR transfer functions. An algorithm for a design of such a controller was proposed.

The new robust guidance law has several important features. First, it assures ZMD for any combination of uncertainties against targets performing any bounded deterministic or random maneuvers. Second, its implementation is simple, since it requires merely a cascade of PD controllers. It should be remarked that, due to the fact that the proposed controller results in high-bandwidth dynamics (which is often the case with robust controllers), its performance is limited by the electro-optical target tracking noise. Systems

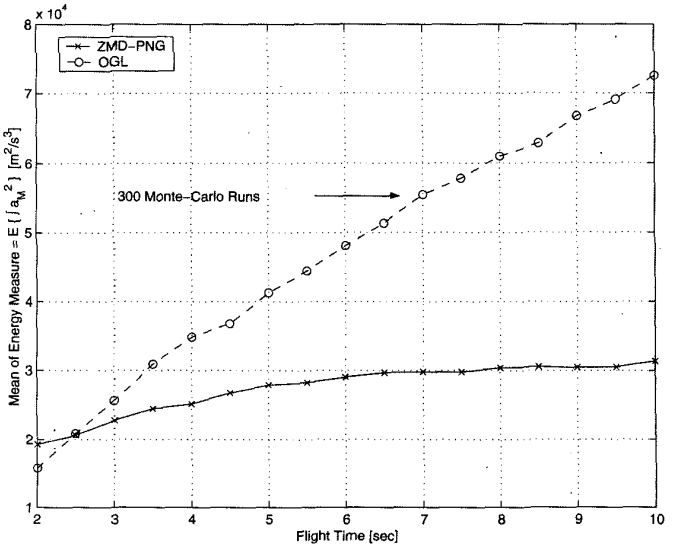

Fig. 6. Mean value of energy expenditure measure, $E\{\int a_M^2\}$ for OGL and ZMD-PNG. Energy expenditure is small.

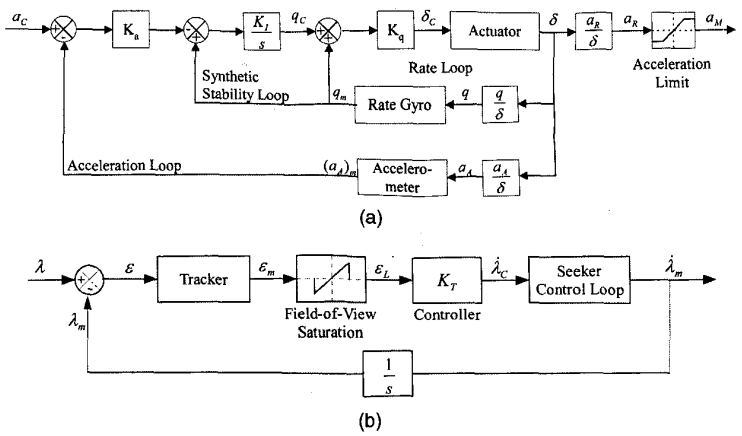

Fig. 7. Block diagrams of (a) flight control system and (b) electro-optical target tracking loop.

having high tracking noise levels, may not constitute a suitable platform for the implementation of the ZMD-PNG. Future research is aimed at deriving suitable robust guidance laws for high-glint and accelerating/decelerating systems.

APPENDIX A. MODEL OF FLIGHT CONTROL SYSTEM

The flight control system was adopted from [22] and is depicted in Fig. 7(a). This pitch-plane three-loop control system comprises a rate loop, a synthetic stability loop, and an accelerometer feedback loop.

The input to the accelerometer feedback loop is the commanded acceleration a_C, which is generated by the guidance law. The output is the required acceleration a_R, which is limited due to aerodynamic or structural constraints, to yield the actual acceleration a_M. The autopilot of this loop is the gain K_A. The feedback signal $(a_A)_m$ is generated by an accelerometer, which is located at the point X_{ACC}, thus sensing the following acceleration magnitude:

$$a_A(t) = a_M(t) + (X_{\text{ACC}} - X_{\text{CG}})\ddot{\theta}(t) \tag{38}$$

where X_{CG} is the location of the center-of-gravity and θ is the body pitch angle.

The signal a_A is the output of the aerodynamic transfer function a_A/δ, with δ being the fin deflection angle. δ is also the output of the body pitch rate control loop, whose input is the commanded pitch rate q_C, generated by the synthetic stability loop [22]. The autopilot of the pitch rate loop is the gain K_q. This gain generates a commanded fin deflection angle δ_C, which constitutes an input to the fin actuators. The aerodynamic transfer function a_R/δ then yields the required output acceleration a_R. The values of the autopilot gains [22] and the other parameters are given in Appendix C.

The aerodynamic model is obtained assuming a short-period approximation. For an axis-symmetric missile, this model yields a fair representation of missile aerodynamic transfer functions both in the pitch and yaw maneuver planes. For illustration, we consider the pitch plane. The equation of moments is

$$S_r Qd \cdot [C_{mq} d/(2V_M) q(t) + C_{m\delta}\delta(t) + C_{m\alpha}\alpha(t)] = J_{yy}\ddot{\theta}(t) \tag{39}$$

where $Q = \rho V_M^2/2$ is the dynamic pressure, ρ is the air density, V_M is missile velocity, S_r is a reference area (the area of the missile cross section), d is the missile diameter, J_{yy} is the pitch moment of inertia, q is the body pitch rate, α is the angle of attack, and $C_{m\alpha}$, $C_{m\delta}$, C_{mq} are the usual stability derivatives.

The equation of forces is given by

$$-S_r \cdot Q \cdot [C_{z\delta} \cdot \delta(t) + C_{z\alpha} \cdot \alpha(t)] = \text{mass} \cdot V_M \cdot \dot{\gamma}(t) \tag{40}$$

where mass is the missile mass, γ is the path angle, and $C_{z\alpha}$, $C_{z\delta}$ are the usual force coefficient derivatives in body axes.

Define

$$\begin{aligned} M_\alpha &\triangleq QS_r dC_{m\alpha}/J_{yy} \\ M_\delta &\triangleq QS_r dC_{m\delta}/J_{yy} \\ M_q &\triangleq QS_r d^2 C_{mq}/(2V_M J_{yy}) \\ Z_\alpha &\triangleq QS_r C_{z\alpha}/(\text{mass} \cdot V_M) \\ Z_\delta &\triangleq QS_r C_{z\delta}/(\text{mass} \cdot V_M) \\ \Delta X &\triangleq X_{\text{CG}} - X_{\text{ACC}} \end{aligned} \tag{41}$$

to obtain the following aerodynamic transfer functions [22]:

$$\frac{a_R}{\delta}(s) = \frac{k_1(n_{12}s^2 + n_{11}s + 1)}{d_{12}s^2 + d_{11}s + 1}$$

$$\frac{a_A}{\delta}(s) = \frac{k_1(n_{22}s^2 + n_{21}s + 1)}{d_{12}s^2 + d_{11}s + 1} \tag{42}$$

$$\frac{q}{\delta}(s) = \frac{k_2(n_{31}s + 1)}{d_{12}s^2 + d_{11}s + 1}$$

where

$$\begin{aligned}
k_1 &= V_M(M_\alpha Z_\delta - M_\delta Z_\alpha)/(M_q Z_\alpha - M_a) \\
k_2 &= k_1/V_M \\
n_{11} &= M_q Z_\delta/(M_\alpha Z_\delta - M_\delta Z_\alpha) \\
n_{12} &= -Z_\delta/(M_\alpha Z_\delta - M_\delta Z_\alpha) \\
n_{21} &= n_{11} + \Delta X k_3/k_1 n_{22} = n_{12} + \Delta X k_3/k_1 \\
n_{31} &= M_\delta/(M_\alpha Z_\delta - M_\delta Z_\alpha) \\
d_{11} &= (M_q + Z_\alpha)/(M_\alpha - M_q Z_\alpha) \\
d_{12} &= 1/(M_q Z_\alpha - M_\alpha).
\end{aligned} \tag{43}$$

The numerical values of the aerodynamic coefficients are given in Appendix C. The coefficients are assumed normally distributed, with mean and standard deviation as given in Appendix C. We proceed with a description of the fin actuator control loop.

The purpose of the fin actuators control loop is to track a commanded fin deflection angle δ_C to yield an actual deflection angle δ. The most commonly used fin actuators control loop model assumes second order dynamics of the form

$$\frac{\delta}{\delta_C} = \frac{K_{\text{servo}}}{s^2/(\omega_{n_{\text{servo}}})^2 + 2 \cdot \zeta_{\text{servo}} \cdot s/\omega_{n_{\text{servo}}} + 1} \tag{44}$$

where $\omega_{n_{\text{servo}}}$ is the natural frequency, ζ_{servo} is a damping coefficient, and K_{servo} is a scale factor.

In practice, the fin actuator control loop is rather complex. First, the control loop is nonlinear, due to acceleration, rate, and position constraints which stem from current, voltage, and mechanical limits, respectively. These limits are given by

$$\begin{aligned}
\delta_L(t) &= \delta_{\max}\text{sat}\left\{\frac{\delta(t)}{\delta_{\max}}\right\} \\
\dot{\delta}_L(t) &= \dot{\delta}_{\max}\text{sat}\left\{\frac{\dot{\delta}(t)}{\dot{\delta}_{\max}}\right\} \\
\ddot{\delta}_L(t) &= \ddot{\delta}_{\max}\text{sat}\left\{\frac{\ddot{\delta}(t)}{\ddot{\delta}_{\max}}\right\}
\end{aligned} \tag{45}$$

where $\delta_{\max}$, $\dot{\delta}_{\max}$, $\ddot{\delta}_{\max}$ are the maximal values of fin angle, rate, and acceleration, respectively. Numerical values are given in Appendix C.

In addition, there are disturbances such as fin bias, denoted δ_B, and fin position measurement noise, denoted n_δ. It is assumed that δ_B is a Gaussian random constant and that n_δ is a zero-mean Gaussian white noise. Numerical values are given in Appendix C.

Our next goal is modeling of the flight control sensors. The missile flight control system uses an accelerometer as a feedback sensor located in the outer acceleration control loop, and a rate gyro in the inner rate control loop. The accelerometer is modeled as follows:

$$(a_A)_m = \frac{K_{\text{ACC}}}{s^2/(\omega_{n_{\text{ACC}}})^2 + 2 \cdot \zeta_{\text{ACC}} \cdot s/\omega_{n_{\text{ACC}}} + 1} a_A + (a_A)_B + n_a \tag{46}$$

where $\omega_{n_{\text{ACC}}}$ is the accelerometer natural frequency, ζ_{ACC} is a damping coefficient, K_{ACC} is a scale factor, $(a_A)_B$ is a measurement bias, assumed a Gaussian constant, and n_a is the measurement noise, assumed zero-mean, white, and Gaussian.

Similarly, the rate gyro model is given by

$$q_m = \frac{K_{\text{RG}}}{s^2/(\omega_{n_{\text{RG}}})^2 + 2 \cdot \zeta_{\text{RG}} \cdot s/\omega_{n_{\text{RG}}} + 1} q + q_B + n_q \tag{47}$$

where $\omega_{n_{\text{RG}}}$ is the natural frequency of the rate gyro, ζ_{RG} is a damping coefficient, K_{RG} is a scale factor, q_B is a measurement bias, assumed a Gaussian constant, and n_q is the measurement noise, assumed zero-mean, white, and Gaussian. Numerical values are given in Appendix C.

APPENDIX B. MODEL OF ELECTRO-OPTICAL TARGET TRACKING LOOP

The purpose of the target tracking loop of an electro-optical missile is to maintain the target within the FOV of a stabilized imaging device, such as a CCD camera. The general layout of such a tracking loop, depicted in Fig. 7(b), was adopted from [10]. This tracking loop is based upon a rate-gyro stabilized platform, where the camera is mounted on gimbals, whose movement is (ideally) isolated from the motion of the missile. The location of the target within FOV limits is measured by an electro-optical tracker, which is an implementation of a correlation algorithm that utilizes the sequence of images generated by the visual motion (the so-called "optical flow"). Thus, the tracker generates a measurement ε_m of the tracking error ε. The FOV is a nonlinear saturation effect of the following form [10]:

$$\text{FOV}(x) \triangleq \begin{cases} x, & |x| \le 1 \\ 0, & |x| > 1 \end{cases}. \tag{48}$$

The resulting tracking error satisfies

$$\varepsilon_L(t) = \varepsilon_{\max}\text{FOV}[\varepsilon_m(t)/\varepsilon_{\max}]. \tag{49}$$

TABLE II
Parameter Values for Illustrative Example

	Parameter/ Disturbance	Units	Mean Value (nominal)	Standard Deviation
Aerodynamics	M_α	$1/s^2$	−250	16.7
	M_δ	$1/s^2$	280	18.7
	Z_α	1/s	−1.6	0.107
	Z_δ	1/s	0.23	0.0153
	M_q	1/s	−1.5	—
	ΔX	m	0.7	—
	V_M	m/s	500	—
	V_C	m/s	1000	—
	μ_0	—	2	—
Autopilot	K_q	s	0.1534	—
	K_a	deg · s/m	0.0007804	—
	K_I	rad/s	13.55	—
Fin actuators	$\omega_{n_{servo}}$	rad/s	200	2
	ζ_{servo}	—	0.6	0.01
	K_{servo}	—	1	0.0167
	δ_B	deg	0	0.167
	n_δ	deg	0	0.0167
	δ_{max}	deg	20	—
	$\dot{\delta}_{max}$	deg/s	230	—
	$\ddot{\delta}_{max}$	deg/s^2	17000	—
Rate gyro	$\omega_{n_{RG}}$	rad/s	300	3
	ζ_{RG}	—	0.65	0.0108
	K_{RG}	—	1	0.0267
	q_B	deg/s	0	0.0667
	n_q	deg/s	0	0.0167
Accelerometer	$\omega_{n_{ACC}}$	rad/s	300	3
	ζ_{ACC}	—	0.65	0.0108
	K_{AC}	—	1	0.0167
	$(a_A)_B$	milli-g	0	1
	n_a	milli-g	0	1
Target tracking loop	τ_T	ms	25	—
	n_ε	mrad	0	0.05
	ε_{max}	deg	1.5	—
	K_T	1/s	10	—
Seeker	$\omega_{n_{seeker}}$	rad/s	150	1.5
	ζ_{seeker}	—	0.7	0.0117
	$\dot{\lambda}_B$	deg/s	0	0.0667
	$n_{\dot{\lambda}}$	deg/s	0	0.0167

The tracking error ε_L is transformed into a commanded LOS rate $\dot{\lambda}_C$ by the tracking loop controller, which is, in our case, the gain K_T (see Fig. 7(b)). The commanded LOS rate constitutes an input to the seeker that generates a measured LOS rate $\dot{\lambda}_m$. This signal is integrated to yield a measured LOS angle λ_m, which is subtracted from the true (kinematic) LOS angle λ to yield the tracking error ε. Since the electro-optical tracker is merely a computational algorithm, it can be best modeled by a pure delay:

$$\varepsilon_m(t) = e^{-s\tau_T}\varepsilon(t) + n_\varepsilon \tag{50}$$

where τ_T is the tracking delay and n_ε is the tracking noise, assumed zero-mean, white, and Gaussian. Numerical values are given in Appendix C.

The seeker is modeled as follows [10]:

$$\dot{\lambda}_m = \frac{1}{s^2/(\omega_{n_{seeker}}^2) + 2\cdot\zeta_{seeker}\cdot s/\omega_{n_{seeker}} + 1}\dot{\lambda}_C + \dot{\lambda}_B + n_{\dot{\lambda}} \tag{51}$$

where as usual $\omega_{n_{seeker}}$ is the natural frequency of the seeker, ζ_{seeker} is the damping coefficient, $\dot{\lambda}_B$ is the LOS rate measurement bias, assumed a Gaussian constant, and $n_{\dot{\lambda}}$ is the LOS rate measurement noise, assumed zero-mean, white, and Gaussian. Numerical values are given in Appendix C.

APPENDIX C. PARAMETER VALUES FOR ILLUSTRATIVE EXAMPLE

Table II contains parameter values that were used in the illustrative example.

REFERENCES

[1] Yaesh, I., and Ben-Asher, J. Z. (1995)
Optimum guidance with a single uncertain time lag.
Journal of Guidance, Control and Dynamics, **18**, 5 (Oct. 1995), 981–988.

[2] Ben-Asher, J. Z., and Yaesh, I. (1990)
Advances in missile guidance theory. .
Progress in Astronautics and Aeronautics, **180** (1990), ch. 6, 141–157.

[3] Yang, C. D., and Chen, H. Y. (1998)
H_∞ robust guidance law for homing missiles.
Journal of Guidance, Control and Dynamics, **21**, 6 (Dec. 1998), 882–890.

[4] Wang. J., Xie, X., Zhong, Y., and Wnag, B. (1997)
H_∞ controller design of a missile guidance and control system.
In *Proccedings of the American Control Conference*, Albuquerque, NM, June 1997, 2779–2780.

[5] Weiss, H., and Hexner, G. (1998)
Modern guidance laws with model mismatch.
In *Proceedings of the IFAC Symposium on Missile Guidance*, Tel-Aviv, Israel, Jan. 1998, 1–12.

[6] Gurfil P., Jodorkovsky, M., and Guelman, M. (1998)
Simple guidance law against highly maneuvering targets.
In *Proceedings of the AIAA Guidance, Navigation and Control Conference*, Boston, MA, Aug. 1998, 570–580.

[7] Gurfil, P., Jodorkovsky, M., and Guelman, M. (2000)
Design of non-saturating guidance systems.
Journal of Guidance, Control and Dynamics, **23**, 4 (July–Aug. 2000), 693–703.

[8] Vicino, A., and Tesi, A. (1993)
Robust strict positive realness: New results for interval plant-controller families.
IEEE Transactions on Automatic Control, **38**, 6 (June 1993), 982–987.

[9] Kogan, J. (1995)
Robust Stability and Convexity—An Introduction.
New York: Springer-Verlag, 1995, ch. 2, 2–13.

[10] Shneydor, N. (1998)
Missile Guidance and Pursuit.
West Sussex, England: Horwood, 1998, ch. 5, 101–124.

[11] Zarchan, P. (1990)
Tactical and strategic missile guidance.
In *Progress in Astronautics and Aeronautics*, **124** (1990), ch. 2, 17–35.

[12] Guelman, M. (1971)
A qualitative study of proportional navigation.
IEEE Transactions on Aerospace and Electronic Systems, **AES-7**, 4 (July 1971), 637–643.

[13] Gurfil, P., Jodorkovsky, M., and Guelman, M. (1998)
Finite time stability approach to proportional navigation systems analysis.
Journal of Guidance, Control and Dynamics, **21**, 6 (Nov. 1998), 853–861.

[14] Zarchan, P. (1979)
Complete statistical analysis of nonlinear missile guidance systems—SLAM.
Journal of Guidance and Control, **2** (Jan. 1979), 71–78.

[15] Dasgupta, S., and Bhagwat, A. S. (1987)
Conditions for designing strictly positive real transfer functions for adaptive output error identification.
IEEE Transactions on Circuits and Systems, **CAS-34**, 7 (July 1987), 731–736.

[16] Sun, W., Khargonekar, P. P., and Shim, D. (1994)
Solution to the positive real control problem for linear time-invariant systems.
IEEE Transactions on Automatic Control, **39**, 10 (Oct. 1994), 2034–2046.

[17] Betser, A., and Zeheb, E. (1993)
Design of robust strictly positive real transfer functions.
IEEE Transactions on Circuits and Systems, **40**, 9 (Sept. 1993), 573–580.

[18] Marquez, H. J., and Damaren, C. J. (1996)
Analysis and synthesis of positive real transfer functions.
Journal of the Franklin Institute, **333B**, 2 (Mar. 1996), 245–256.

[19] Tang, J. G., and Zhou, J. Q. (1995)
On the analysis and synthesis of robust strict positive real systems.
IEEE Transactions on Circuits and Systems, **42**, 9 (Sept. 1995), 553–556.

[20] Shinar, J., Shima, T., and Kebke, A. (1998)
On the validity of linearized analysis in the interception of re-entry vehicles.
In *Proceedings of the 1998 AIAA Guidance, Navigation and Control Conference*, Boston, MA, paper CP-4303.

[21] Ohlmeyer, E. J. (1996)
Root-mean-square miss distance of proportional navigation missile against sinusoidal target.
Journal of Guidance, Control, and Dynamics, **19**, 3 (May–June 1996), 563–568.

[22] Nesline, F. W., and Nesline, M. L. (1984)
Homing missile autopilot response sensitivity to stability derivative variations.
In *Proceedings of the 23rd IEEE Conference on Decision and Control*, Las Vegas, NV, Dec. 1984.

[23] Rusnak, I., and Meir, L. (1991)
Optimal guidance for high order and acceleration constrained missile.
Journal of Guidance, Control and Dynamics, **14**, 3 (May 1991), 589–596.

[24] Rusnak, I. (2000)
Optimal guidance laws with uncertain time-of-flight.
IEEE Transactions on Aerospace and Electronic Systems, **36**, 2 (Apr. 2000), 721–725.

[25] Speyer, J. L. (1976)
An adaptive terminal guidance scheme based on an exponential cost criterion with application to homing missile guidance.
IEEE Transactions on Automatic Control, **AC-21**, 3 (June 1976), 371–375.

[26] Baba Y., Inoue, K., and Howe, R. M. (1998)
Suboptimal guidance with line-of-sight rate only measurements.
Presented at the AIAA Guidance, Navigation and Control Conference, 1998, paper 88-4066-CP.

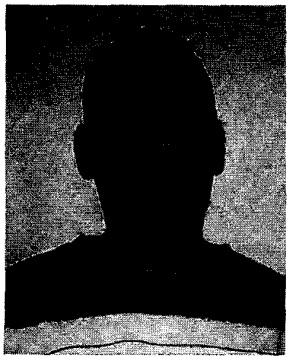

Pini Gurfil received his B.Sc. in 1994, M.S. in 1998, and Ph.D. in 2000, all in aerospace engineering from the Technion, Israel Institute of Technology.

From 1994 to 2000, he was with the Israeli Armament Development Authority, working as a research engineer on advanced tactical missile projects. In July 2000, he assumed a post-doctoral position in the Department of Mechanical and Aerospace Engineering at Princeton University where he is currently a research staff member. His ongoing research activities include global trajectory optimization, spacecraft formation flying, multi-body astrodynamics, vision-based navigation, and robust missile guidance.